TISSUE ENGINEERING: Part A
Volume 20, Numbers 1 and 2, 2014

DOI: 10.1089/ten.tea.2012.0762

Balancing the Rates of New Bone Formation and Polymer Degradation Enhances Healing of Weight-Bearing Allograft/Polyurethane Composites in Rabbit Femoral Defects

Jerald E. Dumas, PhD,[1,2,*,†] Edna M. Prieto, BS,[1,2,*] Katarzyna J. Zienkiewicz, MS,[1] Teja Guda, PhD,[3,4] Joseph C. Wenke, PhD,[4] Jesse Bible, MD,[5] Ginger E. Holt, MD,[5] and Scott A. Guelcher, PhD[1,2,6]

There is a compelling clinical need for bone grafts with initial bone-like mechanical properties that actively remodel for repair of weight-bearing bone defects, such as fractures of the tibial plateau and vertebrae. However, there is a paucity of studies investigating remodeling of weight-bearing bone grafts in preclinical models, and consequently there is limited understanding of the mechanisms by which these grafts remodel *in vivo*. In this study, we investigated the effects of the rates of new bone formation, matrix resorption, and polymer degradation on healing of settable weight-bearing polyurethane/allograft composites in a rabbit femoral condyle defect model. The grafts induced progressive healing *in vivo*, as evidenced by an increase in new bone formation, as well as a decrease in residual allograft and polymer from 6 to 12 weeks. However, the mismatch between the rates of autocatalytic polymer degradation and zero-order (independent of time) new bone formation resulted in incomplete healing in the interior of the composite. Augmentation of the grafts with recombinant human bone morphogenetic protein-2 not only increased the rate of new bone formation, but also altered the degradation mechanism of the polymer to approximate a zero-order process. The consequent matching of the rates of new bone formation and polymer degradation resulted in more extensive healing at later time points in all regions of the graft. These observations underscore the importance of balancing the rates of new bone formation and degradation to promote healing of settable weight-bearing bone grafts that maintain bone-like strength, while actively remodeling.

Introduction

Periarticular fractures involve a weight-bearing joint and often have depressed portions that require extensive open reduction and internal fixation along with subchondral grafting to maintain articular congruence. Maintenance of articular reduction and joint congruity are important for both bone healing and articular alignment, since lack of articular congruence after fractures increases the likelihood of osteoarthritis.[1] While autograft remains the standard of care for bone healing, calcium phosphate (CaP) cements (CPCs) have proven to be superior to autograft for maintaining articular congruence of tibial plateau fractures.[2] A recent retrospective study has reported that 61% of patients treated with buttress plating and autograft experienced loss of reduction after one year compared to 23% of patients treated with hydroxyapatite (HA) bone cement.[3] However, HA bone cement does not extensively remodel and is not replaced by new bone. Moreover, the brittleness and low shear strength of CPCs adversely impact their ability to bear mechanical loads, requiring the use of large, mechanically rigid internal fixation devices (such as buttress plating), which has been suggested to increase complications.[4]

Settable, weight-bearing bone grafts ideally exhibit both initial bone-like mechanical properties and also remodel with minimal resorption gaps such that the strength of the graft exceeds that of host bone during all stages of healing. Injectable bone void fillers (BVFs) include nonsetting allograft[5] and nonallogenic pastes,[6] which are typically delivered using viscous carriers (e.g., sodium hyaluronate,[7] glycerol,[8] or dextran[9]) resulting in weak mechanical properties. Resorbable CPCs,[10–13] such as beta-tricalcium phosphate (β-TCP, slowly resorbed by osteoclasts) or calcium sulfate (CSH) and brushite (undergo dissolution), have also been used to

Departments of [1]Chemical and Biomolecular Engineering, and [6]Biomedical Engineering, Vanderbilt University, Nashville, Tennessee.
[2]Center for Bone Biology, and [5]Department of Orthopaedics and Rehabilitation, Vanderbilt University Medical Center, Nashville, Tennessee.
[3]Department of Biomedical Engineering, University of Texas at San Antonio, San Antonio, Texas.
[4]US Army Institute of Surgical Research, San Antonio, Texas.
*These authors contributed equally to the study.
†*Current affiliation:* Department of Biomedical Engineering, Georgia Institute of Technology/Emory University, Atlanta, Georgia.

enhance bone healing. Tri-phasic CPCs comprising CSH, brushite, and granular β-TCP have been shown to heal metaphyseal defects in preclinical[14] and clinical studies.[15] However, rapid dissolution of CSH and brushite at rates exceeding that of new bone formation can result in loss of mechanical strength,[16] as well as the appearance of a fibrous resorption gap between the ingrowing new bone and the resorbing cement.[17,18] While the initial compressive strength of CPCs is comparable to that of trabecular bone, they undergo brittle fracture at strains less than the yield strain of trabecular bone, resulting in failure due to fatigue under physiologically relevant cyclic loads where the shear component is significant.[6,19] Reinforcement with polymeric, bioactive glass, or ceramic fibers has been reported to enhance the strength and ductility of CPCs, resulting in strengths approaching 50 MPa for poly(lactic-co-glycolic) acid (PLGA) fibers[20] and 130 MPa for magnesium alloy fibers.[21]

Despite the growing interest in weight-bearing settable bone grafts, there is a paucity of studies investigating *in vivo* remodeling in preclinical models. While several studies have reported that weight-bearing grafts heal and form new bone,[22–25] there is limited understanding of the mechanisms by which these grafts remodel *in vivo*, which is essential for designing grafts that ideally maintain bone-like strength during the entire healing process.[26] It has been suggested that the degradation rates of the polymer and ceramic phases must be matched to optimize healing, which is a challenging problem due to the fundamentally different mechanisms by which polymers and ceramics degrade.[26] In this study, we investigated the effects of the rates of new bone formation, matrix resorption, and polymer degradation on healing of settable, weight-bearing polyurethane (PUR) composites comprising approximately equivalent volume fractions of polymer and matrix. Based on our previous study reporting that composites incorporating allograft bone particles (ABPs) remodel by creeping substitution,[22] we investigated ABPs as the reinforcing particulated matrix phase. We hypothesized that matching the rate of new bone formation to that of polymer degradation would optimize healing. To test this hypothesis, we augmented the ABP/PUR composites with either 105 or 420 $\mu g \cdot cm^{-3}$ recombinant human bone morphogenetic protein-2 (rhBMP-2), which was anticipated to increase the rate of new bone formation. Further, rhBMP-2 has been reported to promote zero-order degradation of the PUR network,[27] resulting in more closely balanced rates of bone formation and PUR degradation. The composites were injected into cylindrical defects in the femoral condyles of rabbits and evaluated by micro-computed tomography (μCT) and histomorphometry at 0, 6, and 12 weeks.

Materials and Methods

Materials

LTI-PEG prepolymer (23.6% isocyanate number), poly(ε-caprolactone-*co*-D.L-lactide-*co*-glycolide) triol [162 mg potassium hydroxide/g and $M_n = 1393$ g/mol (measured by gel permeation chromatography)], and rabbit allograft mineralized bone particles (ABPs, 180 ± 70 μm) were received as a gift from Medtronic, Inc.[28] Triethylenediamine (TEDA) catalyst was received as a gift from Goldschmidt, and rhBMP-2 was purchased from R&D Systems. Trehalose dehydrate, heparin sodium salt, acetonitrile, and trifluoroacetic acid (TFA) were purchased from Sigma Aldrich.

Preparation of rhBMP-2

The rhBMP-2 was supplied as a solution comprising 35% acetonitrile and 0.1% TFA. A separate acetonitrile/TFA solution was prepared containing a ratio of 10:1 of trehalose dehydrate:heparin sodium. The rhBMP-2 and trehalose mixtures were combined such that the ratio of rhBMP-2 to trehalose was 1:125. The resulting mixture was distributed in glass vials and frozen at −80°C in preparation for freeze-drying, which produced a powder.

Synthesis of ABP/PUR biocomposites

The appropriate amounts of polyester triol, ABPs, and LTI-PEG prepolymer were added to a mixing cup and mixed by hand for 90 s. The index (ratio of isocyanate:hydroxide equivalents × 100) was 130. The resulting paste and the catalyst (5500 ppm TEDA) were then added to the rhBMP-2 vial and mixed for 60 s. The filler content (ABP and rhBMP-2 powder) was maintained at 70 wt% (56.7 vol%) for each biocomposite (BC) treatment group (Table 1). Two rhBMP-2 doses were investigated: 420 and 105 $\mu g \cdot cm^{-3}$, corresponding to 100% and 25% of the dose recommended for the absorbable collagen sponge (ACS) for rabbits.[29] The porosities of the composites (measured gravimetrically[27]) were 5.7% ± 2.0% (0 μg rhBMP-2 cm^{-3}), 2.7% ± 0.6% (105 μg rhBMP-2 cm^{-3}), and 1.6% ± 0.4% (420 μg rhBMP-2 cm^{-3}).

Rheological properties

The curing profile of the BC without rhBMP-2 ($n = 4$) was determined using a TA Instruments AR2000ex rheometer. The reactive BC was loaded between 25 mm diameter disposable plates and compressed to a gap of 1.5 mm. Measurements of storage (G') and loss (G'') moduli were performed using an oscillatory time sweep method with a frequency of 1 Hz and amplitude of 1% strain. The working time of the BC, defined as the time from the start of mixing until cure, was determined as the $G' - G''$ cross-over point. The flow characteristics of the BC were analyzed by removing the catalyst from the formulation ($n = 3$). Nonsetting samples were poured between 40 mm cross-hatched parallel plates, compressed to a gap of 1.5 mm, and subjected to a dynamic frequency sweep (0.1–100 $rad \cdot s^{-1}$) at 25°C with controlled strain amplitude of 0.02%. A Cox–Merz transformation was applied to the dynamic data to obtain the steady state viscosity (η, Pa·s) as a function of shear rate (γ, s^{-1}). The data were fit to the Herschel–Bulkley model, which relates the viscosity and shear rate of solid-filled suspensions

Table 1. Treatment Groups Evaluated in the Rabbit Femoral Condyle Plug Defect Study

Treatment group	*rhBMP-2 (μg/mL)*	*6 weeks*	*12 weeks*
Empty	0	6	6
ABPs	0	6	6
BC	0	9	10
BC + BMP-L	105	9	10
BC + BMP-H	420	9	8

rhBMP-2, recombinant human bone morphogenetic protein-2; ABPs, allograft bone particles; BC, biocomposite.

with high solids content,[30] to estimate the yield stress (τ_Y, Pa) of the material:

$$\eta = \tau_Y \gamma^{-1} + K\gamma^{(n-1)} \quad (1)$$

where K is the consistency index of the composite (constant) and n is the power-law index of the suspending polymer, which in this case is the nonreactive mixture of polyester triol and LTI-PEG prepolymer.

Mechanical properties

Cylindrical (6-mm diameter) samples of each treatment group were prepared for mechanical testing. The reactive paste was transferred into cylindrical plastic cups and a 1-lb weight (20.7 psi) placed on the material for 10 min. Cylinders were cured in a vacuum oven at 37°C overnight, removed from the plastic cups, and cut using a Buehler saw to a length of 12 mm. After 24 h of hydration in phosphate buffered saline (PBS), the samples were tested using an MTS 898 by preloading to 12 N followed by compression at a rate of 25 mm/min until failure. The original cross-sectional area of the cylinders was used to calculate compressive stress. The ultimate properties reported in this article correspond to the point where maximum stress was achieved. To prepare samples for torsion testing, ~5 mm at each end of 6-mm-diameter cylinders was potted into Technovit 4000 (Heraeus Kulzer) resulting in a central gauge length of about 10 mm. The potting material was prepared by mixing the powder:syrup I:syrup II using a ratio of 2:2:1 following the manufacturer's instructions. After potting, the torsion samples were hydrated for 24 h in PBS, and then tested using an Instron DynaMight 8841 machine equipped with a 1.7 N·m torque cell. The potted ends were gripped using the Instron clamps in a horizontal setup (such that the residual torque was minimal). During testing, the clamps were rotated at an angular speed of 2°/s until failure. The measured torque and rotation angle were used to determine torsional stress using the equation[31,32]:

$$\tau = [\theta(dT/d\theta) + 3T]/(2\pi r^3) \quad (2)$$

where r is the radius of the cylinder, $\theta = \alpha/L$ is the rotation angle per gauge unit length, and T is the measured torque. The derivative $dT/d\theta$ was determined by fitting the T versus θ data to a fifth-order polynomial (between zero up to the maximum torque or ultimate point). Torsional strain (γ) was determined as $\gamma = \theta r$, and the shear modulus calculated from the linear region of the stress–strain curve $G = \tau/\gamma$. Toughness was calculated as the corresponding area under the stress–strain curve from zero to the maximum stress.

Animal study

Forty-two New Zealand White (NZW) rabbits weighing between 3.8 and 4.1 kg were used. All surgical and care procedures were carried out under aseptic conditions per the approved Institutional Animal Care Use Committee (IACUC) protocol. The ABP/PUR putty components were gamma irradiated using a dose of ~25 kGy. Glycopyrrolate was administered at 0.01 mg/kg intramuscularly (IM) followed by ketamine at 40 mg/kg IM. Bilateral defects of ~6 mm diameter by 11 mm in depth were drilled in the lateral metaphysis of the distal femurs of each rabbit. ABP/PUR plugs from each treatment group (Table 1) were subsequently injected into each defect using a 1 mL syringe (modified by cutting the needle hub adapter). Treatment groups for each composite were dispersed randomly among the rabbits with rhBMP-2 treatment groups paired in each rabbit to eliminate systemic effects. The wound was closed ~3 min after injection. The rabbits were euthanized at both 6 and 12 week time points using Fatal-plus (2.2 mL/10 kg) intravenously.

μCT analysis

A μCT40 (SCANCO Medical) was used to acquire images of the extracted femurs post implantation at 6 and 12 weeks. In addition, femurs from NZW rabbits that were part of other experimental protocols which did not affect the skeleton (same age, sex, and similar weight to the rabbits used in this study) were scanned and analyzed as host bone controls. Subsequently, cylindrical defects (6 mm × 11 mm) were created in the host bone controls and filled with the BC formulation. The injected material was left to cure under PBS for 24 h before submerging the bone in formalin for further scanning as BC controls (BC, 0w). μCT scans were performed in formalin at 70 kVp energy, 114 μA source current, 1000 projections per rotation, 300 ms integration time, and an isotropic voxel size of 36 μm. A 0.1-mm-thick aluminum foil filter was employed to reduce beam hardening. Axial images were reconstructed using manufacturer-provided software. Further beam hardening correction was performed during image reconstruction using the manufacturer's 1200 mg·HA·cm^{-3} algorithm. Attenuation values were converted to tissue mineral density (TMD) through calibration with HA phantoms with densities between 0 and 780 mg·HA·cm^{-3} (calibration of the instrument was checked weekly). Using the cortical borders of the defect for alignment, the reconstructed image stack was reoriented such that the depth of the defect was parallel to the z-axis. A radial analysis of the morphometric parameters was conducted from the core of the implant to the interphase with host bone. Four concentric annular volumes of interest with thickness of 1 mm and approximate length of 11 mm (from the outer cortical surface of the femur) were defined for each sample. The three inner regions incorporated the BCs, while the outer region provided information about the interphase with host bone. Ossified tissue was segmented from soft tissue using a threshold of 480 mg·HA·cm^{-3} and Gaussian noise filter settings of sigma 0.2 and support 2. The threshold conditions were chosen visually and kept constant for the analysis of all the samples. Morphometric parameters within the annular volumes were calculated for each region, grouped by treatment and time point, and plotted versus the mean radial distance from the core of the defect R_m [$R_m = (R_o + R_i)/2$, where R_o and R_i correspond to the outer and inner radius of each region, respectively]. Bone volume/total volume (BV/TV), TMD (density of the ossified tissue), connectivity density (Conn.D.), trabecular number (Tb.N.), trabecular thickness (Tb.Th.), and trabecular separation (Tb.Sp.) within the regions of interest were computed using SCANCO's Medical microCT systems software.

Histology and histomorphometry

Rabbit femora were placed in a solution of 10% formalin for 2 weeks followed by a series of ethanol dehydrations. After fixation, the femurs were embedded in poly(methyl methacrylate) and 200-μm sections were cut from the resulting blocks using an Exakt band saw. The sections were

then ground and polished using an Exakt grinding system to <100 μm and stained with Sanderson's rapid bone stain counterstained with van Gieson. Residual ABPs stained light brown, residual polymer stained black, new bone stained pink with dark blue osteocytes within the matrix, red blood cells stained torquiose, and other cells stained a lighter blue. The sections were imaged at 10× magnification with an Olympus camera (DP71) using an Olympus BX60 microscope with and without polarizing the light. Residual ABPs, new bone formation, and remaining polymer were quantified in an area of interest 1.5 mm high × 6 mm wide located in the center of the defect. To analyze the radial remodeling of the scaffolds in time, the rectangular area of interest was further subdivided into three concentric annular regions (each 1 mm thick): A1, representing the area of the defect in contact with the host bone and up to 1 mm away from the edge of the defect; A2, representing the mid-region of the defect; and A3, representing the inner core of the defect. Residual allograft was differentiated from new bone by meeting the following criteria: (i) acellularity, (ii) angular in shape, and (iii) illumination under polarized light. Metamorph (Version 7.0.1) was utilized to perform histomorphometry using a color thresholding and an image layering technique to quantify the number of pixels of each layer and compare it to the total pixels in the area of interest.

Statistical analysis

Three-way analysis of variance (ANOVA), performed in JMP 9.0, was used to determine whether statistical differences existed between treatment groups, area, and time. Comparisons of individual sample groups were performed using a Tukey honestly significant difference (HSD) test. For all experiments $p < 0.05$ was considered statistically significant.

Results

Rheological properties

Figure 1A shows a representative plot of the storage and loss moduli of the BC without rhBMP-2 during cure. The onset of the curve in Figure 1A is delayed due to the time (~9 min) required to set the gap and start data collection after mixing. Initially, the BC exhibits viscoelastic behavior as evidenced by its permanent deformation in response to applied stress, but when the working time is reached (G'–G'' crossover point at 13.7 ± 3.5 min) it becomes more elastomeric. The yield stress τ_Y of a solid-filled suspension can be defined as the minimum stress required for the material to deform.[33] Among the models developed to calculate τ_Y, the Herschel–Bulkley provides the best fit of the data for the nonreactive BC (Fig. 1B). The suspending polymer (0% ABPs) exhibits Newtonian behavior (dotted line) over the range of shear rates investigated (0.1–10 s^{-1}). Consequently, the power-law index n (Eq. 1) of the suspending polymer is equal to unity, and fitting the η versus γ data to the resulting expression results in $\tau_Y = 738$ kPa. Additionally, the viscosity of the material at 5 s^{-1} (the recommended shear rate at which the viscosity of an injectable material should be reported[34]) is 179 kPa·s. The high initial viscosity suggests that the material is not flowable; however, up to the working time the BC can be molded to conform to the contours of the defect.

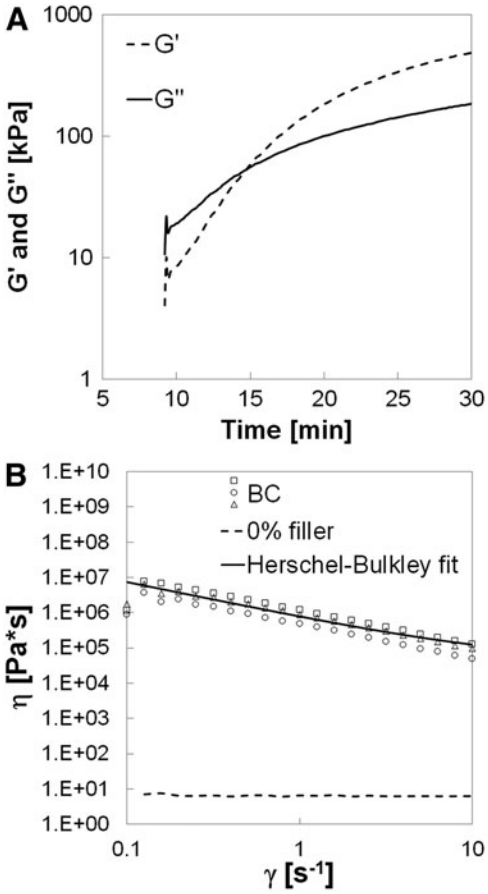

FIG. 1. Rheological properties of the biocomposite (BC) measured by rheometry. **(A)** G' represents the storage modulus and G'' the loss modulus. The G'–G'' crossover point is assumed to be the working time of the BC. **(B)** Viscosity versus shear rate plot illustrating calculation of the yield stress using the Herschel–Bulkley model.

Mechanical properties

Representative compression and torsion stress–strain curves measured for the BCs with and without rhBMP-2 are shown in Figure 2 and compared to a tri-phasic CPC comprising 75% CSH and 25% brushite/granular β-TCP (Pro-Dense®; Wright Medical).[6] The Young's modulus, ultimate stress, ultimate strain, and toughness (area under the stress–strain curve) measured under compression and torsion are listed in Table 2. Under compression, the modulus of the CPC (1689 MPa) was significantly higher compared with the BCs (450–524 MPa), but the strength of the CPC (19.9 MPa) was comparable to that of the BCs (24–28 MPa). However, due to the significantly higher ultimate strain for the BCs (7.4%–8.1%) compared to the CPC (1.7%), the toughness was approximately an order of magnitude greater for the BCs. Addition of rhBMP-2 did not have a significant effect on the mechanical properties of the BCs under compressive loading. Under torsional loading, the modulus of the CPC (2051 MPa) was substantially greater compared with the BCs (40–121 MPa). However, the torsional strength of the CPC (2.9 MPa) was comparable to that of the BCs (1.7–3.6 MPa). Similar to the results for compression, the ultimate strain was dramatically higher for the BCs (4.0%–5.0%) compared to the

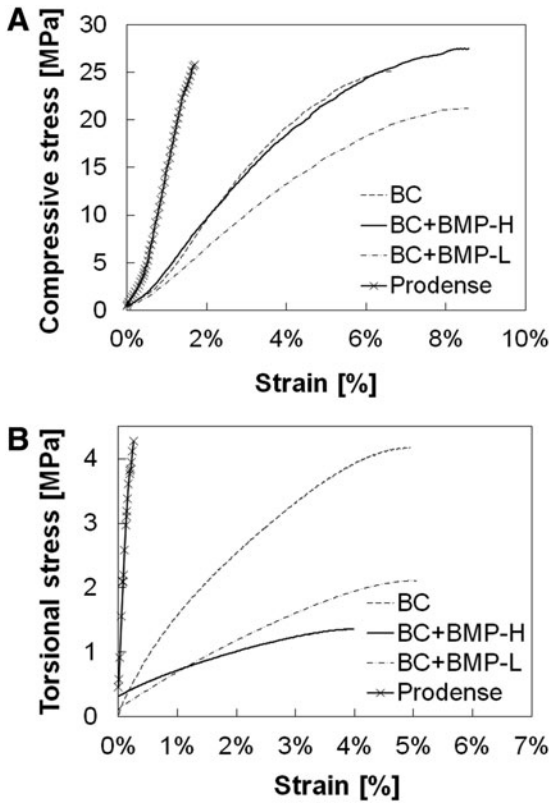

FIG. 2. Representative stress–strain curves for the BCs and calcium phosphate cement. **(A)** Compression. **(B)** Torsion; BMP, bone morphogenetic protein.

CPC (0.2%). Consequently, the toughness was more than an order of magnitude greater for the BCs. In contrast to the results under compression, the torsional properties decreased when rhBMP-2 was added.

μCT data

Representative μCT images of the BC and control groups after 6 and 12 weeks postimplantation are presented in Figure 3. Minimal new bone formation, primarily in the region of the femoral cortex, was observed for the empty and ABP-treated groups at 6 and 12 weeks. These observations suggest that the empty defects did not heal extensively, and that in the absence of the settable PUR binder to maintain the structure of the graft, the allograft particles had resorbed. All BC treatment groups showed evidence of resorption of allograft particles (irregularly shaped bright white particles with sharp edges) and remodeling.

Considering that the BCs remodel by creeping substitution of ABPs initiated at the host bone/BC interface, the radial distribution of key morphometric parameters[35] was measured by μCT as shown in Figure 4. The defect was divided into four annular regions (Fig. 4A) extending for 11 mm and the morphometric parameters BV/TV, TMD, Conn.D., Tb.N., Tb.Th., and Tb.Sp. were measured for each region. The measured parameters of the samples were compared to those of the BC controls (BC, 0w) and healthy host trabecular bone controls (Host bone control). As shown in Figure 4B, TMD showed minimal variation as a function of radial distance, while the values for all groups were slightly higher at 12 weeks compared to 6 weeks. At 6 weeks, BV/TV (Fig. 4C) was relatively constant at ~50 vol% for the BC and BC+BMP-H groups, while BV/TV dropped below 40 vol% in the outer regions (e.g., near the bone/BC interface) of the BC+BMP-L group. By 12 weeks, BV/TV (Fig. 4D) decreased monotonically from the inner core (~50%) to the outer interfacial region (30%–45%) for all groups. At 12 weeks, the BC group showed the largest radial change in BV/TV, ranging from values comparable to the BC control (51% ± 0.4%) at the inner core to values comparable to host trabecular bone (30% + 1%) at the bone-composite interface. None of the groups showed resorption gaps where BV/TV dropped below that of host trabecular bone. In addition to TMD and BV/TV, several standard morphometric parameters,[35] including mean Tb.Th., mean Tb.Sp., Tb.N., and Conn.D., were plotted as a function R_m. Values for each treatment group were compared to measured values for BC controls (0 weeks) and host trabecular bone. As shown in Figure 4E, F, and H, Conn.D., Tb.N., and Tb.Sp. progressed

Table 2. Mechanical Properties of the Injectable Biocomposites and the Calcium Phosphate Cement Measured Under Compressive and Torsional Loads

(A) Compression

Property	*CPC*	*BC*	*BC + BMP-L*	*BC + BMP-H*
Young's modulus (MPa)	1689 ± 197	503 ± 122	452 ± 103	524 ± 68
Stress at failure (MPa)	19.9 ± 5.1	24.0 ± 4.8	24.7 ± 6.4	28.3 ± 3.2
Strain at failure (%)	1.67 ± 0.03	7.39 ± 0.64	8.41 ± 0.11	8.12 ± 0.28
Energy-to-failure ($kJ \cdot m^{-3}$)	168 ± 27	1072 ± 292	1188 ± 180	1395 ± 113

(B) Torsion

Property	*CPC*	*BC*	*BC + BMP-L*	*BC + BMP-H*
Young's modulus (MPa)	2051 ± 45	121 ± 18	56.0 ± 9.5	40.0 ± 6.7
Stress at failure (MPa)	2.90 ± 1.38	3.60 ± 1.05	1.80 ± 0.36	1.70 ± 0.20
Strain at failure (%)	0.20 ± 0.08	5.0 ± 1.2	4.0 ± 0.6	5.0 ± 0.6
Energy-to-failure ($kJ \cdot m^{-3}$)	4.0 ± 3.0	123 ± 53	55.0 ± 16.3	58.0 ± 7.4

Data are reported as the mean ± standard error of the mean (SEM).
CPC, calcium phosphate cement.

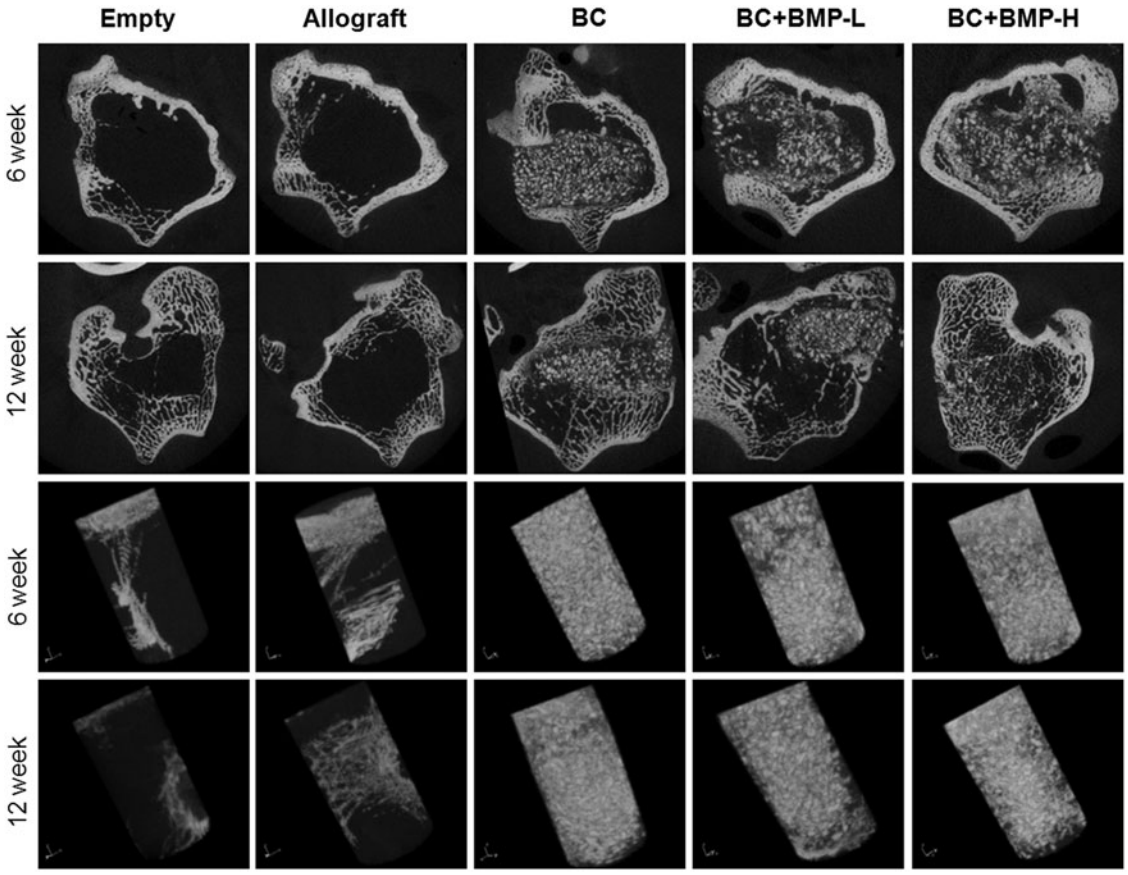

FIG. 3. Representative micro-computed tomography (μCT) images of the empty defects and defects filled with the allograft bone particles, BC, BC + BMP-L, and BC + BMP-H at 6 and 12 weeks. Presented in **(A)** longitudinal sections of the femur and **(B)** as three-dimensional reconstructions of the cylindrical defect region of interest. BMP, bone morphogenetic protein.

monotonically from values comparable to that of the BC control in the inner core region to values comparable to that of the host trabecular bone in the outer annular region. At each point in space and time, the differences between each rhBMP-2 dose were modest. However, values of Conn.D. and Tb.N. decreased from 6 to 12 weeks at each distance and rhBMP-2 dose, while Tb.Sp. increased. Similar to BV/TV, Conn.D., Tb.N., and Tb.Sp. did not drop below values measured for host bone in any region for any of the groups. Interestingly, Tb.Th. exhibited an opposite trend in which the parameter did not converge to the value measured in the host bone as the radial distance increased. Instead, Tb.Th. increased monotonically from values close to that of the BC controls ($201 \pm 4\,\mu m$) in the inner core region to 240–340 μm in the outer annular region compared to $149 \pm 2.6\,\mu m$ for the host bone.

Histology and histomorphometry

Histological sections (Fig. 5) of the empty defects at 6 weeks show minimal new bone formation, which is consistent with the μCT data. However, histological sections of the BC treatment groups (Fig. 6) reveal evidence of cellular infiltration (CI), allograft (A) resorption, and new bone formation (NB). High-magnification views show regions of active remodeling, osteoid formation, appositional growth of new bone on residual allograft particles, and bridging of allograft particles by new bone, suggesting that the BCs remodel by creeping substitution.[22,27,28] In contrast, allograft-treated defects supported minimal ingrowth of new bone, which is consistent with the notion that the continuous polymer phase is essential for supporting new bone formation.

Histomorphometric analysis of each area of interest (labeled A1, A2, and A3 in Fig. 7A) revealed an increase in new bone formation for all groups between 6 and 12 weeks (Fig. 7B–D). Differences over time within a specific area were significant only for A1 in the BC + BMP-L and -H groups, and differences between areas at each time point were not significant for any groups. Area% new bone formation data were fit to the following empirical equation ($R^2 \sim 1$ for all fits):

$$\%B = \frac{at}{(1+bt)} \tag{3}$$

where a and b are fitting parameters (Table 3). In the outer region (A1), $b \to 0$ for all groups, suggesting that ingrowth of new bone near the host bone interface is a zero-order process. Thus, bone forms at an approximately constant rate $r_B = d(\%B)/dt =$ mineral apposition rate, which has been reported as $\sim 4\,\mu m \cdot day^{-1}$ for the distal femur of rabbits.[36] However, $b = 0.307$ in the inner region of group BC (Fig. 7B), indicating that the rate of new bone formation decreased

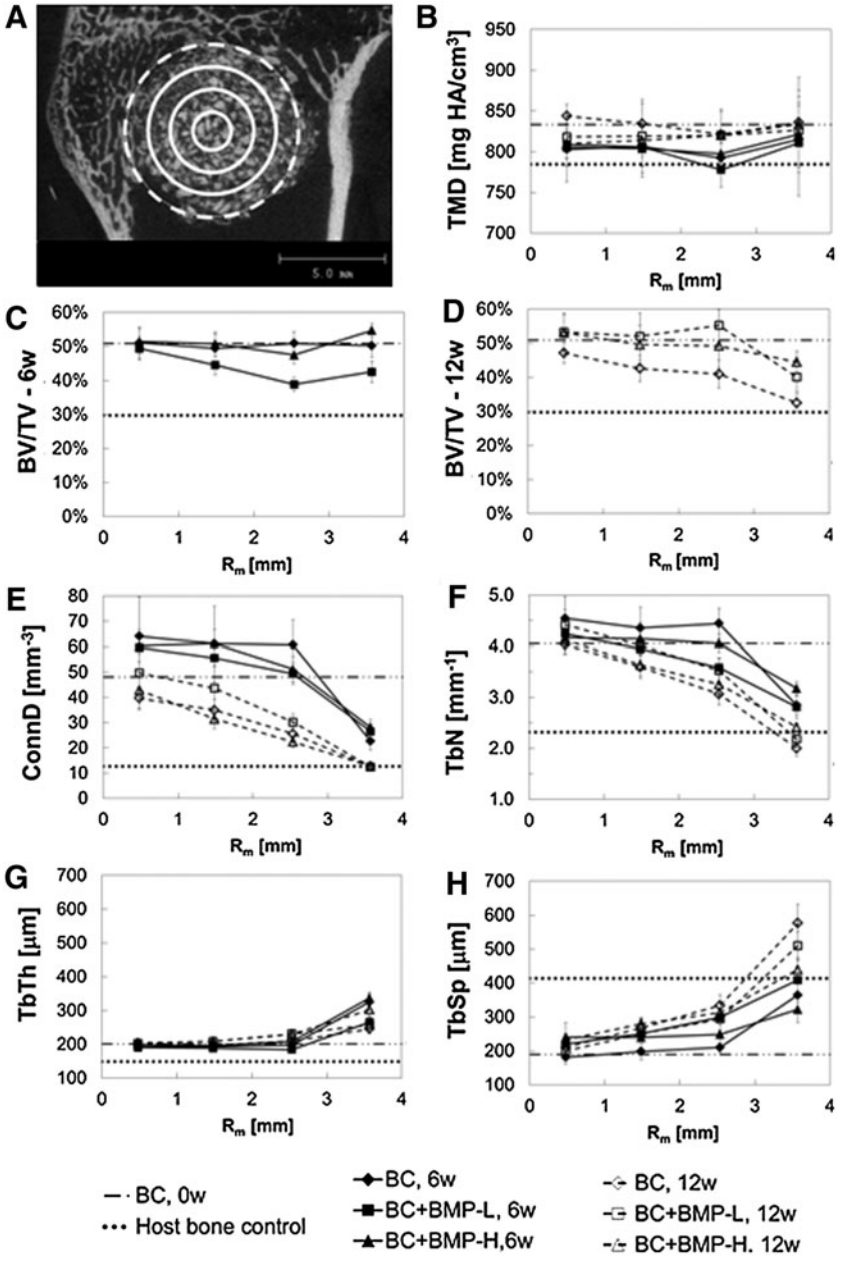

FIG. 4. Radial distribution of morphometric parameters measured by μCT at 6 and 12 weeks. Values of each parameter are compared to those measured for host trabecular bone (dotted line) and the BC controls (0 weeks, dashed line). **(A)** Representative image highlighting subdivision of the defect into four annular shells each 1-mm thick. Morphometric parameters are plotted versus the mean radial distance R_m [$R_m = (R_o + R_i)/2$] of each annular region from the center of the defect. Solid lines delimit regions inside the material, while the dashed line delimits the region near the host bone-composite interface. **(B)** Tissue mineral density (TMD). **(C)** Bone volume/total volume (BV/TV) at 6 weeks. **(D)** BV/TV at 12 weeks. **(E)** Connectivity density (Conn.D.). **(F)** Trabecular number (Tb.N.). **(G)** Trabecular thickness (Tb.Th.). **(H)** Trabecular separation (Tb.Sp).

from 6 to 12 weeks. As anticipated, augmentation with rhBMP-2 significantly increased the rate of new bone formation, but differences between the low and high dose were not significant. In the inner region, the parameter b is lower for the BC + BMP-L (Fig. 7C) and BC + BMP-H (Fig. 7D) groups compared to the BC group, suggesting that the rate of new bone formation in the interior of the graft is decreasing less in the presence of rhBMP-2.

Histomorphometry data for residual allograft are presented for each area in Figure 7E–G. Area% allograft (A) data for the BC group (Fig. 7E) were fit to the following equation:

$$\%A = A_{A,i} - \frac{at}{(1+bt)} \tag{4}$$

where $A_{A,i}$ is the initial area% allograft in the sample at $t = 0$. Values of the fitting parameters a and b for each group are listed in Table 4. As anticipated, for the BC group the area% allograft decreased with time due to osteoclast-mediated resorption,[22,27,28] but the differences between 6 and 12 weeks were not significant for any groups. The half-life varied from 2.3 to 2.9 weeks. In the presence of rhBMP-2, the area% residual allograft was less than in the BC group at 6 weeks, suggesting that rhBMP-2 accelerated allograft resorption at early time points. Interestingly, no significant changes in allograft area% were observed in the rhBMP-2 treatment groups from 6 to 12 weeks. Due to the transient resorption of allograft at 6 weeks, it was not possible to fit the area% allograft data to equation (4) in the presence of rhBMP-2.

Polymer degradation was affected by both time and rhBMP-2 dose (Fig. 7H–J). Differences between 6 and 12 weeks were significant within a specific area for all groups, but differences between areas were not significant. Area%

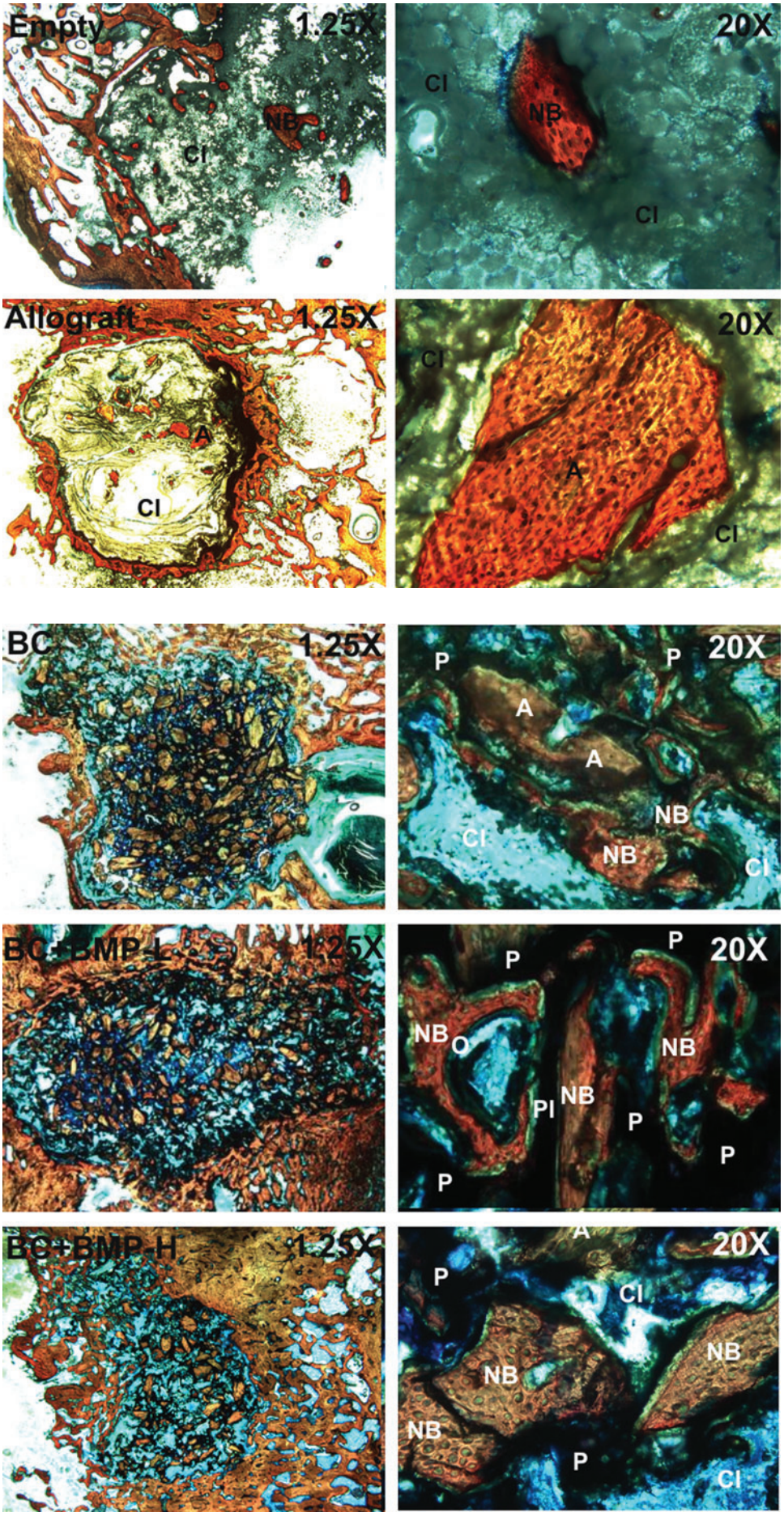

FIG. 5. Low- (1.25×) and high- (20×) magnification images of histological sections of untreated (empty, top) and allograft-filled defects (bottom) at 6 weeks. CI: cellular infiltration, NB: new bone, A: allograft. Color images available online at www.liebertpub.com/tea

FIG. 6. Low- (1.25×) and high- (20×) magnification images of histological sections of the BC (top), BC+ BMP-L (middle), and BC+ BMP-H (bottom) treated defects at 6 and 12 weeks. P, residual polymer; O, osteoid. Color images available online at www.liebertpub.com/tea

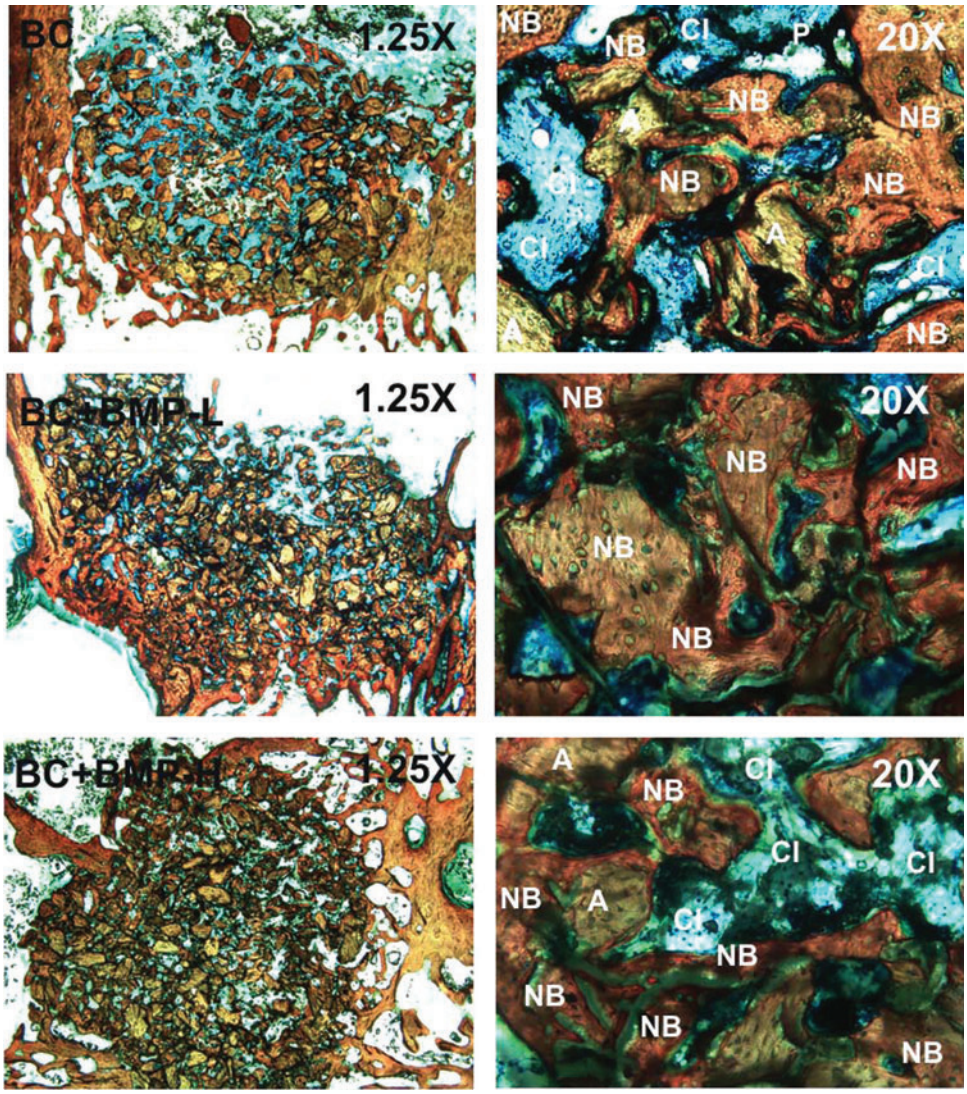

FIG. 6. (Continued).

polymer (P) data for the BC group (Fig. 7H) were fit to the following equation:

$$\%P = A_{P,i} - \alpha \exp^{\beta t} \tag{5}$$

where $A_{P,i}$ is the initial area% polymer in the sample at $t = 0$. The half-life of the polymer ranged from 10.5 to 11.5 weeks, which is substantially longer compared with the allograft but slightly shorter than $t_{1/2} = 14$ weeks reported *in vitro*.[37] Similar to observations from *in vitro* studies, the degradation profile of the poly(ester urethane) is consistent with an autocatalytic mechanism[37] and does not follow the first-order kinetics associated with ester hydrolysis.[38] Local delivery of rhBMP-2 (Fig. 7I, J) changed the shape of the area% polymer curve, which was fit to an equation similar to the one used for new bone:

$$\%P = A_{P,i} - \frac{at}{(1+bt)}. \tag{6}$$

As evidenced by the values of $b \to 0$ (Table 5), the process of PUR degradation in the presence of rhBMP-2 is nearly zero order (i.e., constant rate). Augmentation with rhBMP-2 also accelerated PUR degradation, as evidenced by $t_{1/2} = 6.4$–8.3 weeks for BC + BMP-L and $t_{1/2} = 6.3$–7.5 weeks for BC + BMP-H. Differences in residual polymer were significant between the BC group and the BC + BMP-L and -H groups at 6 weeks, but there were no significant differences between groups at 12 weeks. Thus, rhBMP-2 both altered the mechanism of PUR degradation and also increased the degradation rate.

Discussion

Weight-bearing bone grafts have generated considerable interest in recent years, but the mechanisms by which they remodel, while maintaining their initial bone-like strength are poorly understood. In this study, we investigated the effects of the rate of new bone formation, the rate of reinforcing matrix (allograft) resorption, and the mechanism of polymer degradation on healing of ABP/PUR composites in femoral condyle plug defects in rabbits. The initial compressive strength (24–28 MPa) and toughness (1070–1400 $kJ \cdot m^{-3}$) of the composites were comparable to or exceeding those of trabecular bone (6 MPa and 1050 $kJ \cdot mm^{-3}$,

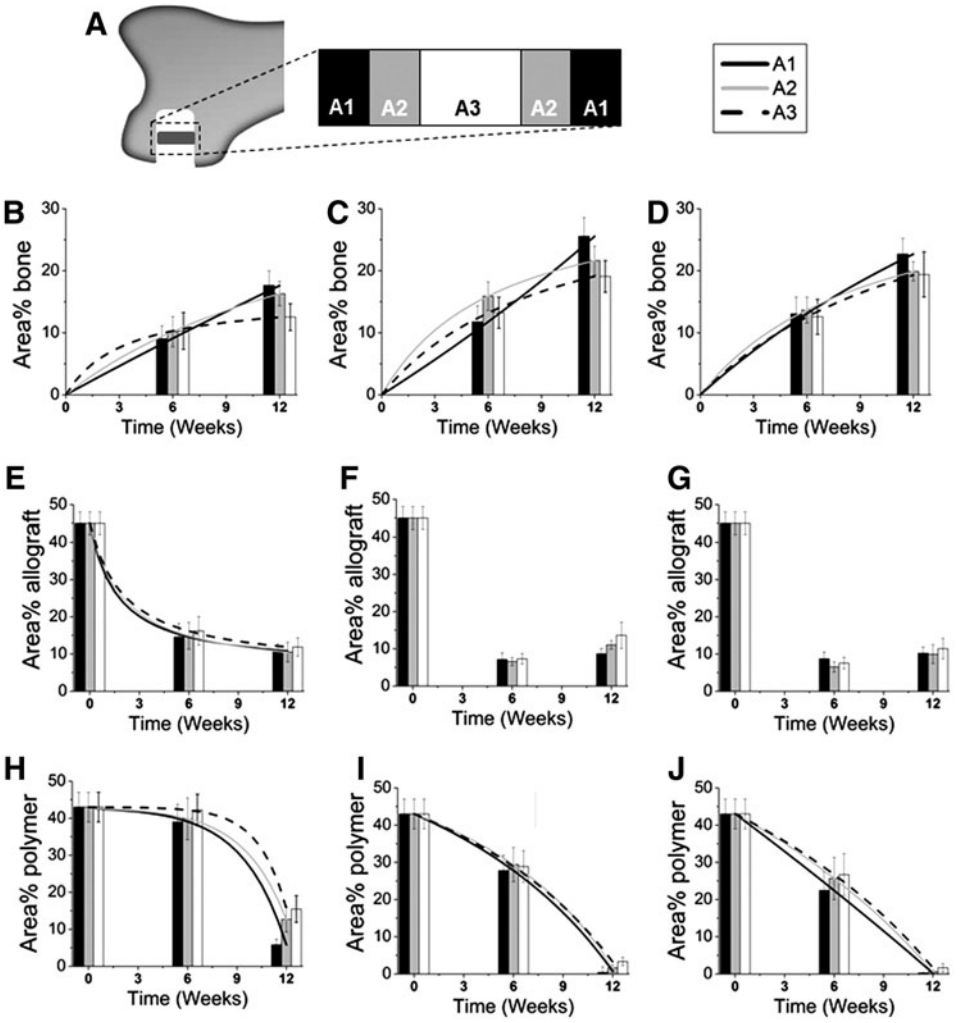

FIG. 7. Histomorphometric evaluation of new bone formation. **(A)** Diagram showing the areas of interest. **(B–D)** Area% new bone measured for **(B)** BC, **(C)** BC + BMP-L, **(D)** BC + BMP-H groups. Data were fit to the function Area% new bone = $at/(1+bt)$ (line). **(E–G)** Area% residual allograft measured for **(E)** BC, **(F)** BC + BMP-L, **(G)** BC + BMP-H groups. Data for BC were fit to the function Area% allograft = $A_{A,i} - at/(1+bt)$ (line), where $A_{A,i}$ is the initial area% allograft. **(H–J)** Area% residual polymer measured for **(H)** BC, **(I)** BC + BMP-L, **(J)** BC + BMP-H groups. Data for BC were fit to the function Area% polymer = $A_{P,i} - \alpha\exp(\beta t)$ (line). Data for the BC + BMP groups were fit to the function Area% allograft = $A_{P,i} - at/(1+bt)$ (line).

respectively[39]). When injected into femoral condyle plug defects in NZW rabbits, new bone formation and healing progressed in the outer region near the host bone interface for up to 12 weeks. Polymer degradation was autocatalytic and new bone formation was approximately zero order, resulting in incomplete healing in the inner regions of the graft at later time points. In contrast, local delivery of rhBMP-2 increased the rate of new bone formation and promoted approximately zero-order degradation of the continuous polymer phase, resulting in improved healing at later time points. Thus, balancing the rates of new bone formation and polymer degradation was observed to improve healing.

Table 3. Fitting Parameters for Bone Histomorphometry Data, Which Were Fit to Area% $B = at/(1+bt)$

	A1		*A2*		*A3*	
Group	a	b	a	b	a	b
BC	1.57	0.0059	2.27	0.0560	4.88	0.307
BC + BMP-L	1.82	−0.0121	5.02	0.149	3.56	0.103
BC + BMP-H	2.58	0.0304	3.66	0.101	3.00	0.072

The settable composites exhibited a working time of 13.7 ± 3.5 min, which is longer than the values of 6–10 min reported for CPCs.[40,41] A proposed criterion for injectability of CPCs dictates that the material can be administered from a syringe by applying a force < 100 N.[6] Consequently, a syringe with diameter > 13 mm would be required to inject the BC due to its high yield stress (738 kPa). The viscosity of the BC at $5\,s^{-1}$ is substantially higher (18×10^3 Pa·s) compared with injectable CPCs (5–10 Pa·s, 35–39 vol% solids[34]). Thus, while the BC has higher initial viscosity and yield stress compared to other BVFs due to its high solids content (57 vol%), it is

Table 4. Fitting Parameters for Allograft Histomorphometry Data, Which Were Fit to Area% $A = A_{A,I} - at/(1+bt)$ for the Biocomposite Group

	A1			*A2*			*A3*		
Group	a	b	$t_{1/2}$ *(week)*	a	b	$t_{1/2}$ *(week)*	a	b	$t_{1/2}$ *(week)*
BC	22.8	0.583	2.3	19.7	0.487	2.6	18.5	0.475	2.9

The parameter $A_{A,i}$ is the initial area% allograft measured by histomorphometry. Data for BC + BMP-L and BC + BMP-H groups could not be accurately fit to the exponential or rational functions.

Table 5. Fitting Parameters for Polymer Histomorphometry Data, Which Were Fit to Area% $P = A_{P,I} - a\tau/(1+b\tau)$ for BC + BMP-L and BC + BMP-H Groups and to Area% $P = A_{P,I} - \alpha \exp(\beta\tau)$ for the BC Group

	A1			*A2*			*A3*		
Group	a (α)	b (β)	$t_{1/2}$ *(week)*	a (α)	b (β)	$t_{1/2}$ *(week)*	a (α)	b (β)	$t_{1/2}$ *(week)*
BC	0.408	0.376	10.5	0.318	0.380	11.0	0.023	0.590	11.5
BC + BMP-L	1.98	−0.0365	6.4	1.69	−0.0425	8.3	1.83	−0.0373	8.2
BC + BMP-H	3.30	−0.0062	6.3	2.44	−0.0258	7.2	2.24	−0.0292	7.5

The parameter $A_{P,i}$ is the initial area% polymer measured by histomorphometry.

moldable and settable within a clinically relevant time frame, which enables the surgeon to conform the graft to the contours of the bone defect.[42]

The initial compressive strength (24.0 ± 4.8 MPa) and modulus (503 ± 122 MPa) of the BCs exceed values reported for trabecular bone, which range from 3.7 to 8.4 MPa and 104 to 300 MPa, respectively.[39,43–45] Similarly, the ultimate strain of the BCs (7.3% ± 0.6%) exceeds that of trabecular bone in human femora (1.05% ± 0.46%)[46], while the toughness ($1072 \pm 292\ kJ \cdot m^{-3}$) is comparable to that of trabecular bone [$1000\ kJ \cdot m^{-3}$([39])]. Under torsional deformation, the strength and modulus of the BCs are 2.9 ± 1.4 and 121 ± 18 MPa, respectively, which are close to values reported for human,[31,47] bovine,[48,49] canine,[43] and ovine[50,51] trabecular bone ranging from 3.1 to 7.7 MPa and 263 to 366 MPa, respectively. However, the ultimate strain of the BC (5.0% ± 1.2%) is comparable to a previous study reporting strain at failure of 4.6% ± 1.3% for trabecular bone.[31] Taken together, these observations suggest that the initial mechanical properties of the BCs are comparable to those of trabecular bone under compression and slightly weaker under torsion.

Recent studies have reported that the poor mechanical properties of CPCs under the physiologically relevant conditions of cyclic loading with a significant shear component[52] limit their use to nonload-bearing applications.[6,19] The weak shear and torsional properties of these materials have been attributed to their inherent brittleness; however, there are limited toughness and fatigue data. Therefore, we compared the toughness of the BCs to an injectable tri-phasic CPC that supports bone healing in both preclinical models[14] and patients.[53] The toughness of the CPC was ~6 times less compared with the BC and trabecular bone under compression, while under torsion the toughness of the CPC was ~30 times less compared with the BC. The reduced toughness of the CPC is attributed, in part, to its lower ultimate strain compared to the BC and trabecular bone under compression (1.7%) and torsion (0.2%). While the area under the stress–strain curve is a convenient estimate of toughness, it is not a true material property,[19] and thus, the fatigue properties, fracture toughness, and/or other measures of reliability (such as the Weibull modulus) must be characterized to assess the potential of the BC to promote healing in weight-bearing bone defects.

While incorporation of CaP has been reported to increase osteoconductivity for some polymers,[54] a recent review has reported that in most studies it does not increase the strength of polymer/ceramic composites.[19] As an exception to this trend, HA/poly(lactic acid) composites incorporating negligible porosity and ~20 vol% HA particles exhibited bending strengths up to 280 MPa. However, since bridging between the ceramic particles and host bone was dependent upon the degradation of poly-L-lactide (PLLA),[55] the rate of remodeling was slow, as evidenced by the fact that 4% of the composite implanted in rabbit femora remained after 7 years.[56] Further, the resorption zone near the host bone interface resulting from phagocytosis of the implant by histocytes[56] is anticipated to reduce its strength. Compression-molded ABP/PUR BCs incorporating 68 vol% ABP exhibited compressive strengths ranging from 100 to 170 MPa and supported extensive cellular infiltration at 6 weeks in rabbit femoral condyle defects.[22] However, only modest new bone formation (~2%) was observed at 6 weeks. The grafts remodeled by creeping substitution, a process characterized by resorption of allograft particles by osteoclasts[27] followed by infiltration of osteoblasts into the newly formed pore.[22,27,28] Subsequent new bone formation was observed on the surfaces of both the polymer and also the residual allograft particles. However, the grafts filled with fibrous tissue due to the lack of a continuous surface for new bone growth. In the present study, the ABP control group with no polymer exhibited extensive resorption of allograft particles and minimal new bone formation away from the cortex. These observations underscore the need for a continuous polymer phase to persist throughout the interior of the BC until an interconnected surface of new bone has formed to sustain healing.

To overcome the limitations of previous studies, settable ABP/PUR composites were designed to incorporate a continuous phase comprising 43% polymer. New bone formation in the outer region of all grafts progressed at a nearly constant rate (Fig. 7B–D). However, $r_B = d(\%B)/dt$ in the inner regions decreased with time, suggesting that mass-transfer limitations associated with infiltration of cells from the host bone into the interior of the scaffold slowed bone formation. A diffusion model for bone formation in scaffolds has been proposed[57]:

$$\frac{\partial c}{\partial t} = \alpha \Delta c \tag{7}$$

where c denotes BV/TV, Δ is the Laplacian, and α ($mm^2 \cdot day^{-1}$) is the scaffold osteoconduction coefficient. Incorporation of ABPs, which resorb by osteoclastic resorption (fast) rather than dissolution (slow), at loadings sufficiently high to present a percolated phase resulted in relatively rapid ($t_{1/2} < 3$ weeks) resorption of the reinforcing matrix. However, the μCT radial analysis (Fig. 4) shows that BV/TV progressed monotonically toward values approaching those of host bone near the interface with no evidence of extensive resorption gaps. These observations point to the potential utilization of α as an independent design parameter that can

be controlled by varying the intrinsic resorption rate and/or loading of the reinforcing matrix.

Local delivery of rhBMP-2 increased the rate of new bone formation and had a transient effect on allograft resorption at 6 weeks. These observations are consistent with *in vitro* and preclinical studies reporting that BMP-2 upregulates osteoclast differentiation and activity[58–61] and drives osteoclast-mediated resorption at high doses.[62] Similar observations have been made for rhBMP-2 released from an ACS implanted in femoral condyle plug defects in sheep.[62] However, transient allograft resorption observed in previous studies has generally been associated with doses of rhBMP-2 considerably higher than the recommended values. Exogenous rhBMP-2 also modified the degradation kinetics of the poly(ester urethane) network.[27,63] While the mechanism of polymer degradation in the presence of rhBMP-2 is not well understood, the drug has been reported to recruit monocytes[64] that degrade lysine-derived PUR scaffolds by an oxidative mechanism.[65] Thus, the observed zero-order polymer degradation kinetics may be macrophage mediated.

The histomorphometry data were further analyzed in Figure 8 to gain insight into the design criteria for weight-bearing bone grafts. The rate of new bone formation r_B relative to the rate of polymer degradation [$r_P = -d(\text{area\% P})/dt$] is plotted versus the parameter f_H, which approximates the fractional healing of the defect:

$$f_H = \frac{\text{area \% bone in defect}}{\text{area \% bone in host bone}}. \quad (8)$$

The area% bone in the host bone was measured by histomorphometry to be 39.3% ± 1.9%. For the BC, at the early stages of healing, $r_B/r_P >> 1$ but it decreased dramatically with time (Fig. 8A). A representative histological section (Fig. 8B) shows poor surface connectivity at 12 weeks, characterized by isolated islands of polymer and allograft. The consequences of mismatched rates of new bone formation and polymer degradation are particularly acute in the inner region, where $r_B/r_P \to 0$ at $f_H = 32\%$ healing, at which time the surface is likely insufficiently interconnected to continue to support cellular infiltration and consequent new bone formation. Thus, autocatalytic degradation of the PUR network driven by pendant carboxylic acid groups formed after hydrolysis of ester bonds does not match the zero-order kinetics of new bone formation,[66] resulting in poor healing in the inner region.

In the presence of exogenous rhBMP-2, the rates of new bone formation and polymer degradation were more balanced. Although r_B/r_P monotonically decreased with time in the presence of rhBMP-2 (Fig. 8C, E), the effect was substantially weaker than in the BC group, and in the outer region r_B/r_P was nearly constant. The relative rate r_B/r_P approached values < 0.2 in the inner regions, but by this time (12 weeks) healing had progressed to $f_H > 50\%$. The representative histological sections from the BC + BMP-L (Fig. 8D) and BC + BMP-H (Fig. 8F) groups show a more connected surface in the inner regions (A2 and A3) for continued bone growth at 12 weeks. Taken together, the data in Figure 8 suggest that to optimize bone healing, the polymer must persist until a sufficient amount of new bone has formed to provide a continuous surface, and that the rate of degradation of the continuous polymeric phase should be matched to the rate of new bone formation. While polyester with a longer half-life[37] is anticipated to delay the onset of rapid polymer degradation until later stages of healing, autocatalytic degradation of polyesters could result in unpredictable outcomes. In contrast, polymers that degrade at a constant rate, for example, by enzymatic degradation, are anticipated to more closely match the rate of new bone formation.[26]

Settable weight-bearing bone grafts could potentially transform the management of tibial plateau fractures, screw augmentation, vertebroplasty, and other orthopedic indications, but their success is predicated on their ability to maintain sufficient bone-like strength actively remodeling. Weight-bearing composites generally comprise a resorbable reinforcing matrix (e.g., short fibers[20,21] or particles[22,56]) dispersed in a continuous phase (e.g., polymers or ceramics). A recent review highlighting the challenges associated with the design of weight-bearing composites has suggested that the rates of degradation of the reinforcing matrix and the

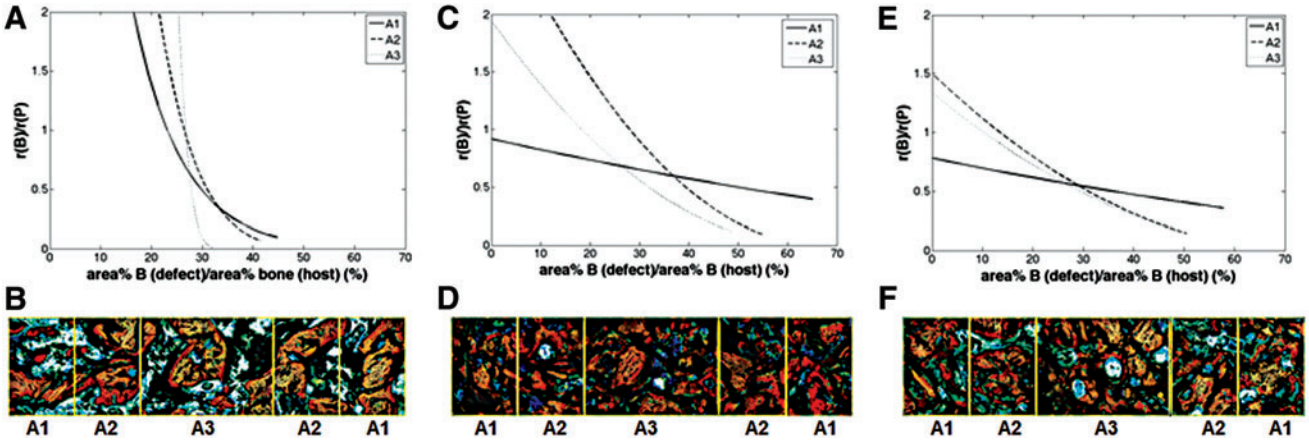

FIG. 8. Analysis of histomorphometric data. The ratio of the rate of new bone formation (r_B) to that of polymer degradation (r_P) was calculated for each group by differentiating the equations expressing area% new bone and area% polymer as a function of time. Representative images of histological sections with highlighted areas of interest are also shown. **(A, B)** BC, **(C, D)** BC + BMP-L, and **(E, F)** BC + BMP-H. Color images available online at www.liebertpub.com/tea

continuous phase should be matched to ensure adequate healing. In this study, we found that early resorption of the reinforcing matrix does not affect healing at later time points, but the continuous phase must persist until sufficient new bone has formed. Hydrolytically degradable polymers undergo autocatalytic degradation, resulting in poor healing in the interior of the graft due to transport limitations associated with ingrowth of new bone.[57] Closely balancing the rates of new bone formation and polymer degradation, accomplished by local delivery of rhBMP-2 in this study, allowed healing to progress to later stages (up to $f_H = 70\%$). A limitation of this study is that none of the areas healed >70% over the 12-week duration. However, our findings point to the importance of both maintaining a continuous surface for bone healing, as well as balancing the rates of new bone formation and continuous phase degradation as a strategy for maintaining sufficient bone-like strength over the lifetime of the graft. Polymers that undergo cell-mediated degradation[26] are anticipated to promote balanced remodeling at all stages of healing, which should be assessed by future long-term studies.

Conclusions

Moldable, settable ABP/PUR BCs exhibited initial mechanical properties comparable to those of trabecular bone. When implanted in plug defects in rabbit femoral condyles, morphometric analysis of both histological sections and μCT reconstructions revealed that new bone formation and healing progressed in both space and time from the outer region near the host bone interface to the inner core for up to 12 weeks. However, the unbalanced rates of autocatalytic polymer degradation and zero-order new bone formation resulted in incomplete healing in the interior of the composite. Augmentation of the composites with rhBMP-2 increased the rate of new bone formation and induced approximately zero-order degradation of the polymer. The consequent balance of new bone formation and polymer degradation resulted in more extensive healing at later time points in all regions of the graft, including the interior. These observations underscore the importance of both maintaining a continuous polymer surface for new bone growth, as well as matching the rate of new bone formation to that of polymer degradation to promote healing of settable weight-bearing bone grafts that maintain bone-like strength, while actively remodeling.

Acknowledgments

Financial support from the Center for Military Biomaterials Research through a subcontract from Rutgers University (W81XWH-04-2-0031) and the National Science Foundation through a CAREER award grant to S.A.G. (DMR-0847711) is gratefully acknowledged. The authors would also like to acknowledge Melinda Higgins for her assistance with the histomorphometric analysis.

Disclosure Statement

No competing financial interests exist.

References

1. Anderson, D.D., Van Hofwegen, C., Marsh, J.L., and Brown, T.D. Is elevated contact stress predictive of post-traumatic osteoarthritis for imprecisely reduced tibial plafond fractures? J Orthop Res **29,** 33, 2011. Epub 2010/07/08.
2. Russell, T.A., and Leighton, R.K. Comparison of autogenous bone graft and endothermic calcium phosphate cement for defect augmentation in tibial plateau fractures. A multicenter, prospective, randomized study. J Bone Joint Surg Am **90,** 2057, 2008. Epub 2008/10/03.
3. Simpson, D., and Keating, J.F. Outcome of tibial plateau fractures managed with calcium phosphate cement. Injury **35,** 913, 2004. Epub 2004/08/11.
4. Hall, J.A., Beuerlein, M.J., and McKee, M.D. Open reduction and internal fixation compared with circular fixator application for bicondylar tibial plateau fractures. Surgical technique. J Bone Joint Surg Am **91 Suppl 2 (Pt 1),** 74, 2009. Epub 2009/03/11.
5. Schwartz, Z., Goldstein, M., Raviv, E., Hirsch, A., Ranly, D.M., and Boyan, B.D. Clinical evaluation of demineralized bone allograft in a hyaluronic acid carrier for sinus lift augmentation in humans: a computed tomography and histomorphometric study. Clin Oral Implants Res **18,** 204, 2007. Epub 2007/03/14.
6. Bohner, M. Design of ceramic-based cements and putties for bone graft substitution. Eur Cell Mater **20,** 1, 2010. Epub 2010/06/25.
7. Chazono, M., Tanaka, T., Komaki, H., and Fujii, K. Bone formation and bioresorption after implantation of injectable beta-tricalcium phosphate granules-hyaluronate complex in rabbit bone defects. J Biomed Mater Res A **70,** 542, 2004. Epub 2004/08/13.
8. Cammisa, F.P., Jr., Lowery, G., Garfin, S.R., Geisler, F.H., Klara, P.M., McGuire, R.A., *et al.* Two-year fusion rate equivalency between Grafton DBM gel and autograft in posterolateral spine fusion: a prospective controlled trial employing a side-by-side comparison in the same patient. Spine (Phila Pa 1976) **29,** 660, 2004. Epub 2004/03/12.
9. Chan, C., Thompson, I., Robinson, P., Wilson, J., and Hench, L. Evaluation of Bioglass/dextran composite as a bone graft substitute. Int J Oral Maxillofac Surg **31,** 73, 2002. Epub 2002/04/09.
10. Friedman, C.D., Constantino, P.D., Takagi, S., and Chow, L.C. BoneSource™ hydroxyapatite cement: a novel biomaterial for craniofacial skeletal tissue engineering and reconstruction. J Biomed Mater Res **43,** 428, 1998.
11. Chim, H., and Gosain, A.K. Biomaterials in craniofacial surgery experimental studies and clinical application. J Craniofac Surg **20,** 29, 2009.
12. Gasparini, G., Boniello, R., Moro, A., Tamburrini, G., Di Rocco, C., and Pelo, S. Cranial reshaping using methyl methacrylate: technical note. J Craniofac Surg **20,** 184, 2009.
13. Moreira-Gonzalez, A., Jackson, I.T., Miyawaki, T., Barakat, K., and DiNick, V. Clinical outcome in cranioplasty: critical review in long-term follow-up. J Craniofac Surg **14,** 144, 2003.
14. Urban, R.M., Turner, T.M., Hall, D.J., Inoue, N., and Gitelis, S. Increased bone formation using calcium sulfate-calcium phosphate composite graft. Clin Orthop Relat Res **459,** 110, 2007. Epub 2007/04/07.
15. Gitelis, S., Urban, R.M., Turner, T.M., Heck, R., and Parameswaran, A.D., editors. Outcomes in the Treatment of Benign Bone Lesions Using an Engineering Ceramic: Preclinical and Clinical Results. Materials and Processes for Medical Devices Conference; August 10–12, 2009; Minneapolis, MN.
16. Ikenaga, M., Hardouin, P., Lemaitre, J., Andrianjatovo, H., and Flautre, B. Biomechanical characterization of a biode-

gradable calcium phosphate hydraulic cement: a comparison with porous biphasic calcium phosphate ceramics. J Biomed Mater Res **40,** 139, 1998. Epub 1998/03/25.
17. Urban, R.M., Turner, T.M., Hall, D.J., Infanger, S., Cheema, N., and Lim, T.H. Healing of large defects treated with calcium sulfate pellets containing demineralized bone matrix particles. Orthopedics **26(5 Suppl),** s581, 2003. Epub 2003/05/21.
18. Greish, Y.E., and Brown, P.W. Phase evolution during the formation of stoichiometric hydroxyapatite at 37.4 degrees C. J Biomed Mater Res B Appl Biomater **67,** 632, 2003. Epub 2003/10/07.
19. Wagoner Johnson, A.J., and Herschler, B.A. A review of the mechanical behavior of CaP and CaP/polymer composites for applications in bone replacement and repair. Acta Biomater **7,** 16, 2011. Epub 2010/07/27.
20. Kruger, R., and Groll, J. Fiber reinforced calcium phosphate cements—on the way to degradable load bearing bone substitutes? Biomaterials **33,** 5887, 2012. Epub 2012/05/29.
21. Kruger, R., Seitz, J.M., Ewald, A., Bach, F.W., and Groll, J. Strong and tough magnesium wire reinforced phosphate cement composites for load-bearing bone replacement. J Mech Behav Biomed Mater **20,** 36, 2013. Epub 2013/03/05.
22. Dumas, J.E., Davis, T.E., Yoshii, T., Nyman, J., Holt, G.E., Perrien, D.S., *et al.* Synthesis of allograft bone/polymer composites and evaluation of remodeling in a rabbit femoral condyle model. Acta Biomater **6,** 2394, 2010.
23. Lian, Q., Li, D.C., He, J.K., and Wang, Z. Mechanical properties and *in-vivo* performance of calcium phosphate cement-chitosan fibre composite. Proc Inst Mech Eng [H] **222,** 347, 2008. Epub 2008/05/22.
24. Kim, J., McBride, S., Fulmer, M., Harten, R., Garza, Z., Dean, D.D., *et al.* Fiber-reinforced calcium phosphate cement formulations for cranioplasty applications: a 52-week duration preclinical rabbit calvaria study. J Biomed Mater Res B Appl Biomater **100,** 1170, 2012. Epub 2011/11/25.
25. Pan, Z., and Jiang, P. Assessment of the suitability of a new composite as a bone defect filler in a rabbit model. J Tissue Eng Regen Med **2,** 347, 2008. Epub 2008/07/10.
26. Jones, J.R. Review of bioactive glass: from Hench to hybrids. Acta Biomater **9,** 4457, 2013. Epub 2012/08/28.
27. Dumas, J.E., Brownbaer, P.B., Prieto, E.M., Guda, T., Hale, R.G., Wenke, J.C., *et al.* Injectable reactive biocomposites for bone healing in critical-size rabbit calvarial defects. Biomed Mater **7,** 024112, 2012. Epub 2012/03/30.
28. Dumas, J.E., Zienkiewicz, K., Tanner, S.A., Prieto, E.M., Bhattacharyya, S., and Guelcher, S. Synthesis and characterization of an injectable allograft bone/polymer composite bone void filler with tunable mechanical properties. Tissue Eng Part A **16,** 2505, 2010. Epub 2010/03/12.
29. Smith, D.M., Afifi, A.M., Cooper, G.M., Mooney, M.P., Marra, K.G., and Losee, J.E. BMP-2-based repair of large-scale calvarial defects in an experimental model: regenerative surgery in cranioplasty. J Craniofac Surg **19,** 1315, 2008. Epub 2008/09/25.
30. Poslinski, A.J., Ryan, M.E., Gupta, R.K., Seshadri, S.G., and Frechette, F.J. Rheological behavior of filled polymeric systems. I. Yield stress and shear-thinning effects. J Rheol **32,** 703, 1988.
31. Bruyere Garnier, K., Dumas, R., Rumelhart, C., and Arlot, M.E. Mechanical characterization in shear of human femoral cancellous bone: torsion and shear tests. Med Eng Phys **21,** 641, 1999. Epub 2000/03/04.
32. Ford, C.M., and Keaveny, T.M. The dependence of shear failure properties of trabecular bone on apparent density and trabecular orientation. J Biomech **29,** 1309, 1996. Epub 1996/10/01.
33. Carreau, P.J., and Lavoie, P.A. Rheological properties of filled polymers. Macromol Symp **108,** 111, 1996.
34. Baroud, G., Cayer, E., and Bohner, M. Rheological characterization of concentrated aqueous beta-tricalcium phosphate suspensions: the effect of liquid-to-powder ratio, milling time, and additives. Acta Biomater **1,** 357, 2005. Epub 2006/05/17.
35. Bouxsein, M.L., Boyd, S.K., Christiansen, B.A., Guldberg, R.E., Jepsen, K.J., and Muller, R. Guidelines for assessment of bone microstructure in rodents using micro-computed tomography. J Bone Miner Res **25,** 1468, 2010. Epub 2010/06/10.
36. Cacchioli, A., Ravanetti, F., Soliani, L., and Borghetti, P. Preliminary study on the mineral apposition rate in distal femoral epiphysis of New Zealand white rabbit at skeletal maturity. Anat Histol Embryol **41,** 163, 2012. Epub 2011/12/14.
37. Hafeman, A., Li, B., Yoshii, T., Zienkiewicz, K., Davidson, J., and Guelcher, S. Injectable biodegradable polyurethane scaffolds with release of platelet-derived growth factor for tissue repair and regeneration. Pharm Res **25,** 2387, 2008.
38. Lehtonen, T.J., Tuominen, J.U., and Hiekkanen, E. Resorbable composites with bioresorbable glass fibers for load-bearing applications. *In vitro* degradation and degradation mechanism. Acta Biomater **9,** 4868, 2013. Epub 2012/09/12.
39. Allen, M.R., Hogan, H.A., Hobbs, W.A., Koivuniemi, A.S., Koivuniemi, M.C., and Burr, D.B. Raloxifene enhances material-level mechanical properties of femoral cortical and trabecular bone. Endocrinology **148,** 3908, 2007. Epub 2007/05/05.
40. Lewis, G. Percutaneous vertebroplasty and kyphoplasty for the stand-alone augmentation of osteoporosis-induced vertebral compression fractures: present status and future directions. J Biomed Mater Res B Appl Biomater **81B,** 371, 2007.
41. Clarkin, O.M., Boyd, D., Madigan, S., and Towler, M.R. Comparison of an experimental bone cement with a commercial control, Hydroset™. J Mater Sci Mater Med **20,** 1563, 2009.
42. Kretlow, J.D., Young, S., Klouda, L., Wong, M., and Mikos, A.G. Injectable biomaterials for regenerating complex craniofacial tissues. Adv Mater Deerfield **21,** 3368, 2009. Epub 2009/09/15.
43. Eswaran, S.K., Allen, M.R., Burr, D.B., and Keaveny, T.M. A computational assessment of the independent contribution of changes in canine trabecular bone volume fraction and microarchitecture to increased bone strength with suppression of bone turnover. J Biomech **40,** 3424, 2007. Epub 2007/07/10.
44. Morgan, E.F., and Keaveny, T.M. Dependence of yield strain of human trabecular bone on anatomic site. J Biomech **34,** 569, 2001. Epub 2001/04/20.
45. Du, C., Ma, H., Ruo, M., Zhang, Z., Yu, X., and Zeng, Y. An experimental study on the biomechanical properties of the cancellous bones of distal femur. Biomed Mater Eng **16,** 215, 2006. Epub 2006/03/07.
46. Burgers, T.A., Mason, J., Niebur, G., and Ploeg, H.L. Compressive properties of trabecular bone in the distal femur. J Biomech **41,** 1077, 2008. Epub 2008/01/22.
47. Halawa, M., Lee, A.J., Ling, R.S., and Vangala, S.S. The shear strength of trabecular bone from the femur, and some factors affecting the shear strength of the cement-bone interface. Arch Orthop Trauma Surg **92,** 19, 1978. Epub 1978/08/11.

48. Stone, J.L., Beaupre, G.S., and Hayes, W.C. Multiaxial strength characteristics of trabecular bone. J Biomech **16,** 743, 1983. Epub 1983/01/01.
49. Ashman, R.B., Corin, J.D., and Turner, C.H. Elastic properties of cancellous bone: measurement by an ultrasonic technique. J Biomech **20,** 979, 1987. Epub 1987/01/01.
50. Mitton, D., Rumelhart, C., Hans, D., and Meunier, P.J. The effects of density and test conditions on measured compression and shear strength of cancellous bone from the lumbar vertebrae of ewes. Med Eng Phys **19,** 464, 1997. Epub 1997/07/01.
51. Kasra, M., and Grynpas, M.D. On shear properties of trabecular bone under torsional loading: effects of bone marrow and strain rate. J Biomech **40,** 2898, 2007. Epub 2007/04/24.
52. Gisep, A., Kugler, S., Wahl, D., and Rahn, B. Mechanical characterisation of a bone defect model filled with ceramic cements. J Mater Sci Mater Med **15,** 1065, 2004. Epub 2004/11/02.
53. Watson, J.T., Borrelli, J., Weber, T.G., Choplin, R.H., Persohn, S.A., White, R., *et al.*, editors. A prospective functional analysis of proximal tibia fractures using a calcium sulfate/calcium phosphate composite graft with an early weight bearing protocol. Orthopaedic Trauma Association, Baltimore, MD, 2010.
54. Kim, S.S., Sun Park, M., Jeon, O., Yong Choi, C., and Kim, B.S. Poly(lactide-co-glycolide)/hydroxyapatite composite scaffolds for bone tissue engineering. Biomaterials **27,** 1399, 2006. Epub 2005/09/20.
55. Shikinami, Y., Matsusue, Y., and Nakamura, T. The complete process of bioresorption and bone replacement using devices made of forged composites of raw hydroxyapatite particles/poly l-lactide (F-u-HA/PLLA). Biomaterials **26,** 5542, 2005.
56. Hasegawa, S., Ishii, S., Tamura, J., Furukawa, T., Neo, M., Matsusue, M., *et al.* A 5–7 year *in vivo* study of high-strength hydroxyapatite/poly(L-lactide) composite rods for the internal fixation of bone fractures. Biomaterials **27,** 1327, 2006.
57. Roshan-Ghias, A., Vogel, A., Rakotomanana, L., and Pioletti, D.P. Prediction of spatio-temporal bone formation in scaffold by diffusion equation. Biomaterials **32,** 7006, 2011. Epub 2011/06/28.
58. Smoljanovic, T., Bojanic, I., Bicanic, G., and Delimar, D. Re; Toth, J.M., Boden, S.D., Burkus, J.K., *et al.* Short-term osteoclastic activity induced by locally high concentrations of recombinant human bone morphogenetic protein-2 in a cancellous bone environment. Spine **34,** 539, 2009; Spine (Phila Pa 1976) **35,** 597, 2010; author reply −8. Epub 2010/03/02.
59. Jensen, E.D., Pham, L., Billington, C.J., Jr., Espe, K., Carlson, A.E., Westendorf, J.J., *et al.* Bone morphogenic protein 2 directly enhances differentiation of murine osteoclast precursors. J Cell Biochem **109,** 672, 2010. Epub 2009/12/30.
60. Kaneko, H., Arakawa, T., Mano, H., Kaneda, T., Ogasawara, A., Nakagawa, M., *et al.* Direct stimulation of osteoclastic bone resorption by bone morphogenetic protein (BMP)-2 and expression of BMP receptors in mature osteoclasts. Bone **27,** 479, 2000. Epub 2000/10/18.
61. Itoh, K., Udagawa, N., Katagiri, T., Iemura, S., Ueno, N., Yasuda, H., *et al.* Bone morphogenetic protein 2 stimulates osteoclast differentiation and survival supported by receptor activator of nuclear factor-kappaB ligand. Endocrinology **142,** 3656, 2001. Epub 2001/07/19.
62. Toth, J.M., Boden, S.D., Burkus, J.K., Badura, J.M., Peckham, S.M., and McKay, W.F. Short-term osteoclastic activity induced by locally high concentrations of recombinant human bone morphogenetic protein-2 in a cancellous bone environment. Spine (Phila Pa 1976) **34,** 539, 2009. Epub 2009/02/26.
63. Wu, G., Liu, Y., Iizuka, T., and Hunziker, E.B. The effect of a slow mode of BMP-2 delivery on the inflammatory response provoked by bone-defect-filling polymeric scaffolds. Biomaterials **31,** 7485, 2010. Epub 2010/07/20.
64. Cunningham, N.S., Paralkar, V., and Reddi, A.H. Osteogenin and recombinant bone morphogenetic protein 2B are chemotactic for human monocytes and stimulate transforming growth factor beta-1 mRNA expression. Proc Natl Acad Sci U S A **89 (December),** 11740, 1992.
65. Hafeman, A.E., Zienkiewicz, K.J., Zachman, A.L., Sung, H.J., Nanney, L.B., Davidson, J.M., *et al.* Characterization of the degradation mechanisms of lysine-derived aliphatic poly(ester urethane) scaffolds. Biomaterials **32,** 419, 2011. Epub 2010/09/25.
66. Eglin, D., Mortisen, D., and Alini, M. Degradation of synthetic polymeric scaffolds for bone and cartilage tissue repairs. Soft Matter **5,** 938, 2009.

Address correspondence to:
Scott A. Guelcher, PhD
Department of Chemical and Biomolecular Engineering
Vanderbilt University
PMB 351604
2301 Vanderbilt Place
Nashville, TN 37235-1604

E-mail: scott.guelcher@vanderbilt.edu

Received: December 24, 2012
Accepted: July 17, 2013
Online Publication Date: October 3, 2013